

**Reduction in Depth for a Radiating Flange Backed by a  
Rectangular Resonant Cavity Using High Index Materials:  
Preliminary Report**

by Gregory A. Mitchell

ARL-MR-0851

September 2013

## **NOTICES**

### **Disclaimers**

The findings in this report are not to be construed as an official Department of the Army position unless so designated by other authorized documents.

Citation of manufacturer's or trade names does not constitute an official endorsement or approval of the use thereof.

Destroy this report when it is no longer needed. Do not return it to the originator.

# **Army Research Laboratory**

Adelphi, MD 20783-1197

---

---

**ARL-MR-0851**

**September 2013**

---

## **Reduction in Depth for a Radiating Flange Backed by a Rectangular Resonant Cavity Using High Index Materials: Preliminary Report**

**Gregory A. Mitchell**

**Sensors and Electron Devices Directorate, ARL**

## REPORT DOCUMENTATION PAGE

*Form Approved*  
OMB No. 0704-0188

Public reporting burden for this collection of information is estimated to average 1 hour per response, including the time for reviewing instructions, searching existing data sources, gathering and maintaining the data needed, and completing and reviewing the collection information. Send comments regarding this burden estimate or any other aspect of this collection of information, including suggestions for reducing the burden, to Department of Defense, Washington Headquarters Services, Directorate for Information Operations and Reports (0704-0188), 1215 Jefferson Davis Highway, Suite 1204, Arlington, VA 22202-4302. Respondents should be aware that notwithstanding any other provision of law, no person shall be subject to any penalty for failing to comply with a collection of information if it does not display a currently valid OMB control number.

**PLEASE DO NOT RETURN YOUR FORM TO THE ABOVE ADDRESS.**

<b>1. REPORT DATE (DD-MM-YYYY)</b> September 2013	<b>2. REPORT TYPE</b> Final	<b>3. DATES COVERED (From - To)</b> May to August 2013	
<b>4. TITLE AND SUBTITLE</b> Reduction in Depth for a Radiating Flange Backed by a Rectangular Resonant Cavity Using High Index Materials: Preliminary Report		<b>5a. CONTRACT NUMBER</b>	
		<b>5b. GRANT NUMBER</b>	
		<b>5c. PROGRAM ELEMENT NUMBER</b>	
<b>6. AUTHOR(S)</b> Gregory A. Mitchell		<b>5d. PROJECT NUMBER</b> 6362.1	
		<b>5e. TASK NUMBER</b>	
		<b>5f. WORK UNIT NUMBER</b>	
<b>7. PERFORMING ORGANIZATION NAME(S) AND ADDRESS(ES)</b> U.S. Army Research Laboratory ATTN: RDRL-SER-M 2800 Powder Mill Road Adelphi MD 20783-1197		<b>8. PERFORMING ORGANIZATION REPORT NUMBER</b>  ARL-MR-0851	
		<b>10. SPONSOR/MONITOR'S ACRONYM(S)</b>	
<b>9. SPONSORING/MONITORING AGENCY NAME(S) AND ADDRESS(ES)</b>		<b>11. SPONSOR/MONITOR'S REPORT NUMBER(S)</b>	
<b>12. DISTRIBUTION/AVAILABILITY STATEMENT</b> Approved for public release; distribution unlimited.			
<b>13. SUPPLEMENTARY NOTES</b>			
<b>14. ABSTRACT</b> Resonant cavities are widely used to enhance the properties of antennas' far-field radiation characteristics. However, at low frequencies, the depth of these cavities can become excessively large making them unusable in many applications. The arrival of metamaterials exhibiting high permittivity and permeability with relatively low loss at these frequencies allows designers to potentially load a resonant cavity to greatly reduce the depth of such structures. This report uses numerical simulations to investigate how loading a resonant rectangular cavity with high index metamaterials affects the broadband performance of an antenna in terms of realized gain. Both isotropic and anisotropic materials are investigated and the benefits and detractors of all cases are outlined.			
<b>15. SUBJECT TERMS</b> Infinite flange, rectangular waveguide, high index material			
<b>16. SECURITY CLASSIFICATION OF:</b>			<b>17. LIMITATION OF ABSTRACT</b>  UU
<b>a. REPORT</b> Unclassified	<b>b. ABSTRACT</b> Unclassified	<b>c. THIS PAGE</b> Unclassified	
			<b>18. NUMBER OF PAGES</b>  30
<b>19a. NAME OF RESPONSIBLE PERSON</b> Gregory Mitchell			
			<b>19b. TELEPHONE NUMBER (Include area code)</b> (301) 394-2322

Standard Form 298 (Rev. 8/98)  
Prescribed by ANSI Std. Z39.18

---

## Contents

---

<b>List of Figures</b>	<b>iv</b>
<b>List of Tables</b>	<b>v</b>
<b>1. Introduction</b>	<b>1</b>
<b>2. Rectangular Cavity Filled with Vacuum</b>	<b>1</b>
2.1 Cylindrical Probe.....	2
2.2 Flat Rectangular Probe .....	4
<b>3. Rectangular Cavity Loaded with High Index Material</b>	<b>6</b>
3.1 Isotropic Materials.....	7
3.1.1 Dielectric Materials .....	8
3.1.2 Magnetic Materials.....	10
3.1.3 Magneto-Dielectric Material .....	10
3.2 Anisotropic Materials .....	11
3.2.1 Dominant Axis in the X-Direction .....	12
3.2.2 Dominant Axis in the Y-Direction .....	15
3.3.3 Dominant Axis in the Z-Direction.....	16
3.4 Dominant Axes in the $\mu_x$ and $\epsilon_y$ Directions.....	17
3.5 Dominant Axes in the $\mu_x$ and $\mu_z$ Directions.....	18
<b>4. Conclusions</b>	<b>19</b>
<b>5. Path Forward</b>	<b>20</b>
<b>6. References</b>	<b>21</b>
<b>Distribution List</b>	<b>22</b>

---

## List of Figures

---

Figure 1. Empty rectangular cavity with infinite flange fed by a cylindrical bare probe. ....	2
Figure 2. VSWR for rectangular cavity fed by flat cylindrical probe. ....	3
Figure 3. Realized gain for rectangular cavity fed by flat cylindrical probe. ....	4
Figure 4. Empty rectangular cavity with infinite flange fed by a flat rectangular bare probe. ....	4
Figure 5. VSWR for rectangular cavity fed by flat rectangular probe. ....	5
Figure 6. Realized gain for rectangular cavity fed by flat rectangular probe. ....	6
Figure 7. Illustration of the variable dimensions of a tapered rectangular cavity with constant cutoff frequency. ....	8
Figure 8. Realized gain with $\epsilon_r = 10$ and $\mu_r = 1$ . ....	9
Figure 9. Return loss with $\epsilon_r = 10$ and $\mu_r = 1$ . ....	9
Figure 10. Realized gain with $\epsilon_r = 1$ and $\mu_r = 10$ . ....	10
Figure 11. Realized gain with $\epsilon_r = \sqrt{10}$ and $\mu_r = \sqrt{10}$ . ....	11
Figure 12. Realized gain with $\epsilon_x = 10$ , $\epsilon_y = 1$ , $\epsilon_z = 1$ , $\mu_x = 1$ , $\mu_y = 1$ , and $\mu_z = 1$ . ....	12
Figure 13. Realized gain for tapered cavity with dimensions given in table 4 with $\epsilon_x = 1$ , $\epsilon_y =$ $1$ , $\epsilon_z = 1$ , $\mu_x = 10$ , $\mu_y = 1$ , and $\mu_z = 1$ . ....	12
Figure 14. Realized gain with $\epsilon_x = 1$ , $\epsilon_y = 1$ , $\epsilon_z = 1$ , $\mu_y = 1$ , and $\mu_z = 1$ . Run 5 has $\mu_x = 15$ while run 8 has $\mu_x = 20$ . ....	13
Figure 15. VSWR with $\epsilon_x = 1$ , $\epsilon_y = 1$ , $\epsilon_z = 1$ , $\mu_y = 1$ , and $\mu_z = 1$ . Run 5 has $\mu_x = 15$ while run 8 has $\mu_x = 20$ . ....	14
Figure 16. Realized gain with $\epsilon_x = 1$ , $\epsilon_y = 10$ , $\epsilon_z = 1$ , $\mu_x = 1$ , $\mu_y = 1$ , and $\mu_z = 1$ . ....	15
Figure 17. Realized gain with $\epsilon_x = 1$ , $\epsilon_y = 1$ , $\epsilon_z = 1$ , $\mu_x = 1$ , $\mu_y = 10$ , and $\mu_z = 1$ . ....	16
Figure 18. Realized gain with $\epsilon_x = 1$ , $\epsilon_y = 1$ , $\epsilon_z = 10$ , $\mu_x = 1$ , $\mu_y = 1$ , and $\mu_z = 1$ . ....	16
Figure 19. Realized gain with $\epsilon_x = 1$ , $\epsilon_y = 1$ , $\epsilon_z = 1$ , $\mu_x = 1$ , $\mu_y = 1$ , and $\mu_z = 10$ . ....	17
Figure 20. Realized gain with $\epsilon_x = 1$ , $\epsilon_y = 10$ , $\epsilon_z = 1$ , $\mu_x = 10$ , $\mu_y = 1$ , and $\mu_z = 1$ . ....	18
Figure 21. Realized gain with $\epsilon_x = 1$ , $\epsilon_y = 1$ , $\epsilon_z = 1$ , $\mu_x = 15$ , $\mu_y = 1$ , and $\mu_z = 10$ . ....	19

---

## List of Tables

---

Table 1. Dimensions of the cavity parameters corresponding to figure 2 in inches. ....	3
Table 2. Dimensions of the parameters for a resonant cavity fed by a flat probe corresponding to figures 5 and 6 in inches. ....	5
Table 3. Cavity dimensions for figures 6 and 7 in. ....	6
Table 4. Cavity dimensions for figure 8 in inches. ....	13
Table 5. Cavity dimensions for figures 11 and 12 in inches. ....	14

INTENTIONALLY LEFT BLANK.

---

## 1. Introduction

---

An open-ended rectangular waveguide in the form of a radiating structure has many practical applications in communications and radar, and has been studied extensively in a variety of methods (1–4). However, with the advent of high index metamaterials, the design space for such structures in the very high frequency (VHF)/ultra high frequency (UHF) bands has become of greater interest. Especially with the arrival of magnetic materials that exhibit low enough propagation losses to bring them into the realm of high frequency applications. By loading a rectangular resonating cavity with high index materials, the front-to-back-ratio of the cavity has the potential to be reduced over the VHF/UHF bands while still achieving a positive realized gain. This opens up a whole new area of potential low profile applications for cavity backed apertures.

This report investigates the designs of a flanged rectangular resonating cavity loaded with various high index materials. The band of interest for this report is 200–500 MHz. All materials in this preliminary report are assumed to be lossless, and the figure of merit to be used is the far-field realized gain of the radiating structure. All simulations have been run using the time domain solver of CST Studio Suite 2012, and adaptive meshing has been used to verify convergence in the far-field results.

---

## 2. Rectangular Cavity Filled with Vacuum

---

A coaxial feed has long been used to stimulate electric and magnetic fields within a rectangular waveguide. This coaxial-to-waveguide junction has been widely studied, and many successful methods have been developed. Generally a coaxial input is fed into the center of the widest transverse waveguide dimension near the aperture, and a conducting probe is used to stimulate the dominant mode within the rectangular waveguide (5, 6). For a rectangular waveguide this is the transverse electric ( $TE_{10}$ ) mode. Sometimes the probe is a bare conductor and sometimes it is wrapped in a dielectric barrier. In our approach, we use similar feeding techniques to attempt to achieve a broadband match for our resonating cavity; however, we are placing the probe close to the aperture. This may not allow enough distance for additional modes to fully attenuate leading to additional modes at the aperture. Using a half loop feed may help alleviate this problem, but that is not covered in this report.

The first example in this report re-creates this approach to show a baseline of performance over the 200–500 MHz frequency band, but also to show how this results in a large back cavity that would be unusable in a low profile situation.

## 2.1 Cylindrical Probe

Figure 1 shows an empty cavity fed by a SMA coaxial input connected to a bare cylindrical probe. This probe can be represented by a perfect electric conductor (PEC). Since the frequency band of interest is 200–500 MHz, the transverse dimension of the aperture in the longest direction must be at least  $a = 0.5\lambda_o$ , where  $\lambda_o$  is the free space wavelength at 200 MHz. In practice, it would be a good idea to make the cutoff frequency lower than 200 MHz, because behavior right at the cutoff frequency becomes unpredictable. Any smaller than this and the dominant mode will not be allowed to propagate inside the cavity at this frequency. The shorter dimension is chosen here as  $b = a/2.25$ . The depth of the cavity from the probe is known as the backshort. This varies with frequency; however, it is generally closest to or slightly less than  $0.25\lambda_g$ , where  $\lambda_g$  is the guide wavelength at some frequency. In practice, the frequency used to calculate the guide wavelength for a broadband radiating cavity is near the center frequency of the band.

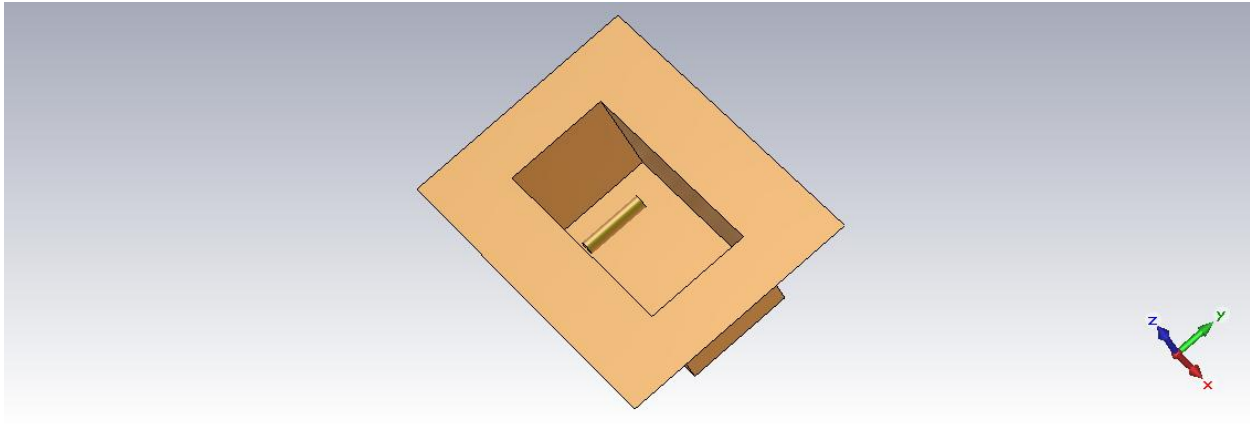


Figure 1. Empty rectangular cavity with infinite flange fed by a cylindrical bare probe.

Figure 2 shows the vertical standing wave ratio (VSWR) for the dimensions listed in table 1. As we can see, this VSWR stays below 2.6 for the majority of the band for all three of these runs. These dimensions yielded the best VSWR across the band out of several simulations altering the probe length ( $L$ ), radius of the cylindrical probe, the backshort in terms of guide wavelength, and the distance of the probe from the aperture. The high VSWR from 200–210 MHz in run 2 may be alleviated by increasing the size of  $a$  in the x-direction slightly above  $0.5\lambda_o$ . Generally, a VSWR below 2 is considered good for a broadband match, but a VSWR of 2.5 is still acceptable.

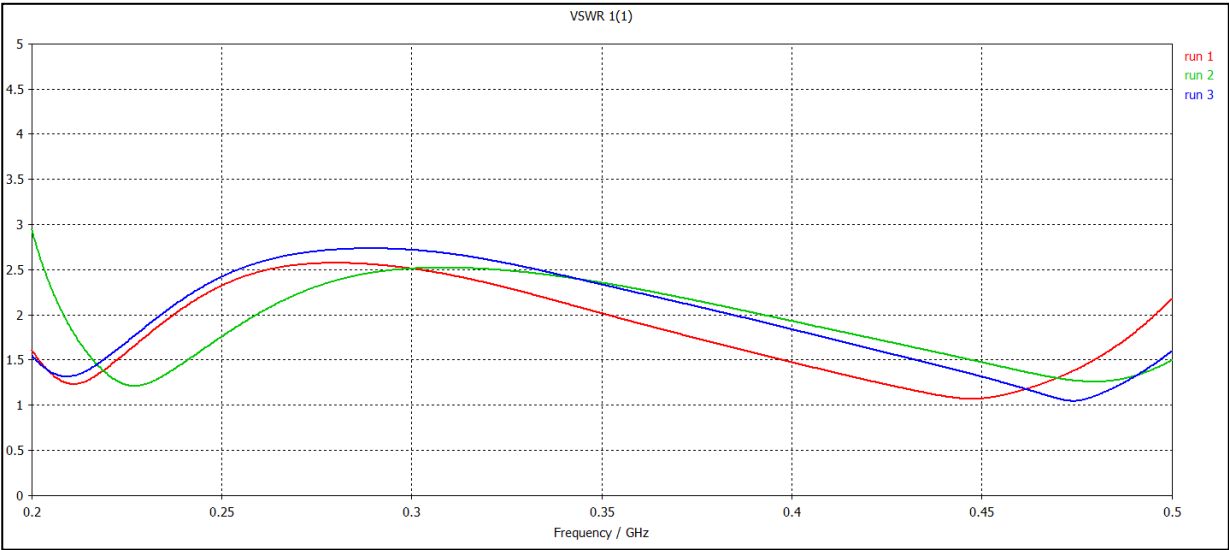


Figure 2. VSWR for rectangular cavity fed by flat cylindrical probe.

Table 1. Dimensions of the cavity parameters corresponding to figure 2 in inches.

Run No.	Backshort	a	b	Probe Radius	L	Distance From Aperture
1	10.2	29.5	13.1	0.92	8.5	1
2	10.2	29.5	13.1	1.1	7.2	1.1
3	10.2	29.5	13.1	1.1	8.5	1.1

Figure 3 shows the realized gain for the dimensions listed in table 1. Since the radiating aperture is large and the VSWR indicates a good broadband match, we see a good realized gain over the band as well.

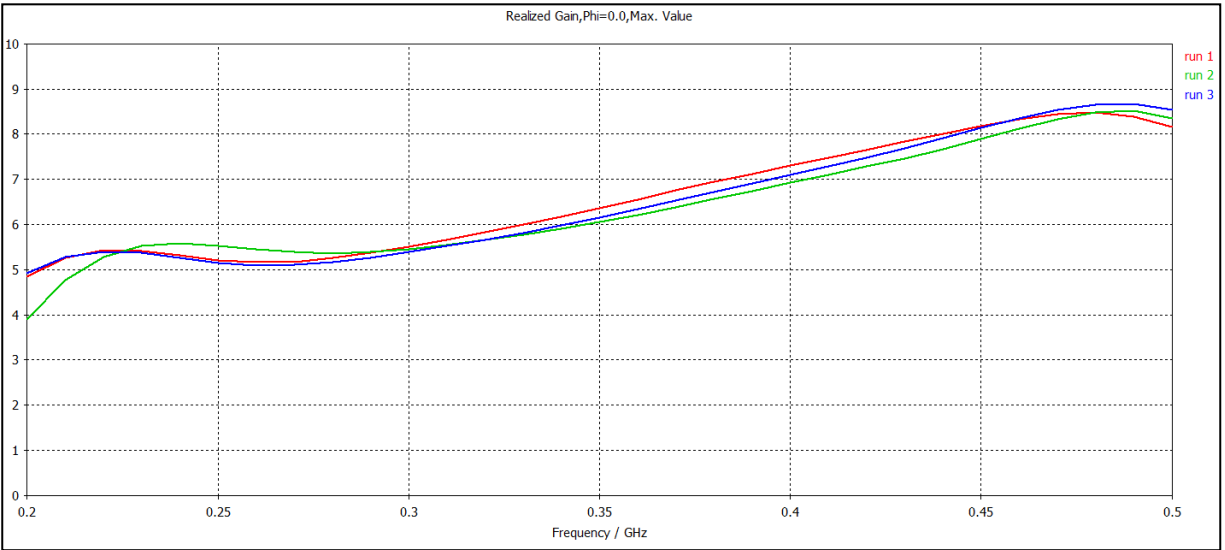


Figure 3. Realized gain for rectangular cavity fed by flat cylindrical probe.

### 2.2 Flat Rectangular Probe

Figure 4 shows an empty cavity fed by a SMA coaxial input connected to a flat bare rectangular probe. This cavity has the same transverse dimensions  $a = 0.5\lambda_0$  and  $b = a/2.25$  as in figure 1. The cylindrical probe added additional thickness in the form of the probe radius to the depth of the cavity. Originally the width of the probe (PW) was to be the same as the radius of the cylinder. However, to improve the match at the input by changing the width of the flat probe, we can change the impedance, much like a transmission line.

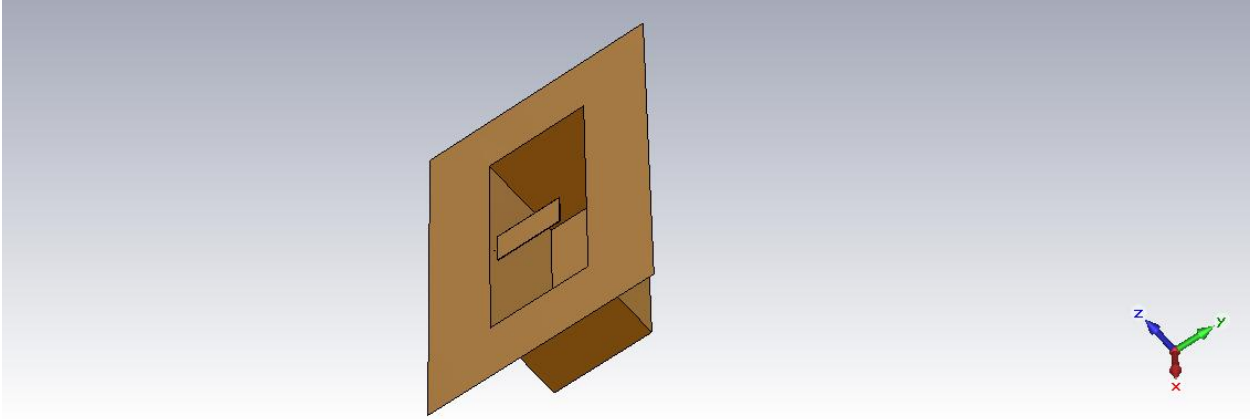


Figure 4. Empty rectangular cavity with infinite flange fed by a flat rectangular bare probe.

Figure 5 shows the VSWR for the dimensions listed in table 2. The VSWR achieved by using the flat probe in figure 4 has a better broadband match than that of the cylindrical probe in figure 1.

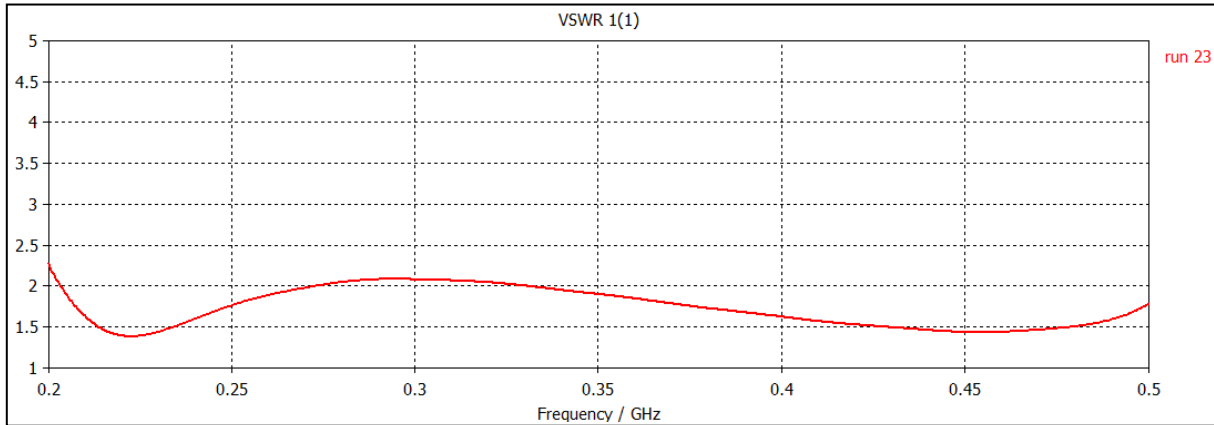


Figure 5. VSWR for rectangular cavity fed by flat rectangular probe.

Table 2. Dimensions of the parameters for a resonant cavity fed by a flat probe corresponding to figures 5 and 6 in inches.

<b>Backshort</b>	<b>a</b>	<b>b</b>	<b>PW</b>	<b>L</b>	<b>Distance From Aperture</b>
10.2	29.5	13.1	4.3	8.5	0.84

Figure 6 shows the realized gain for the dimensions listed in table 2. Since the radiating aperture is the same size as that of figure 1 and the VSWR is improved, we see an increase in the realized gain over the band as well. The flat probe has allowed us to reduce the broadband VSWR while allowing for a reduction in cavity depth of 25.3 mm or approximately 1.0 in.

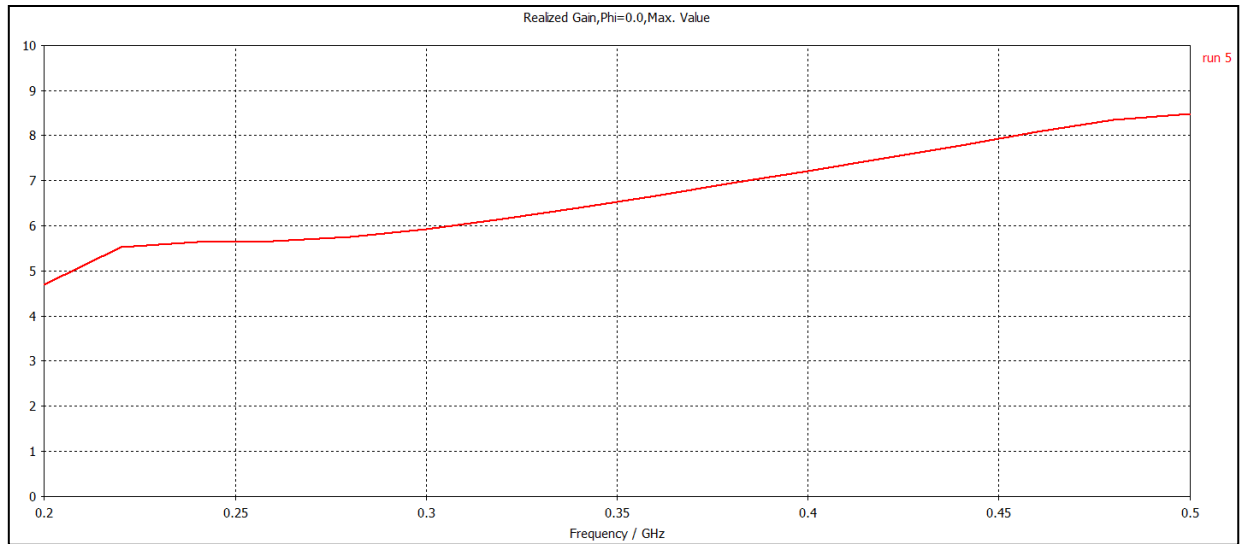


Figure 6. Realized gain for rectangular cavity fed by flat rectangular probe.

### 3. Rectangular Cavity Loaded with High Index Material

This section attempts to illustrate the differences in performance for a resonating cavity with a backshort loaded with high index materials. Since ultimately the high index material of interest has both dielectric and magnetic properties, we explore materials with both  $\epsilon_r > 1$  and  $\mu_r > 1$ . Both isotropic materials and anisotropic materials are examined in order to demonstrate the benefits of being able to control the directions of  $\epsilon_r$  and  $\mu_r$  in an anisotropic tensor. In terms of general application, we desire to keep the radiating aperture  $2 \text{ ft}^2$  or smaller while reducing the total depth of the cavity to 2 in or less.

All cavity dimensions in the following analyses are based on the dimensions listed in table 3, unless otherwise noted. The dimensions of  $a_0$  and  $b$  yield a radiated aperture size of  $2.9 \text{ ft}^2$ . This is quite a bit larger than our target size of  $2 \text{ ft}^2$ , but the results demonstrate why the aperture size needs to be so large except for in a few specific cases.

Table 3. Cavity dimensions for figures 6 and 7 in.

$a_0$	$b$	$a_1$	$f_c$ (MHz)	$d$	$\delta$	PW
30.68	13.64	9.7	192.5	4.1	0.27	0.7

### 3.1 Isotropic Materials

When  $\epsilon_r > 1$  and  $\mu_r > 1$  this will lower the cutoff frequency by the equation

$$f_c = \frac{c}{1 \times 10^6 \lambda_o \sqrt{\epsilon_r \mu_r}} \quad (1)$$

where  $c$  is the speed of light in (m/s<sup>2</sup>),  $\lambda_o$  is the free space wavelength at the desired cutoff frequency in meters, and  $f_c$  is the cutoff frequency in MHz. Therefore, by increasing the permittivity or permeability of the material in the backshort of the cavity, we can reduce the depth in figures 1 and 4, but we are introducing additional propagating modes besides the dominant TE<sub>10</sub> mode. Therefore, we must taper the cavity inversely to the material such that  $f_c$  remains constant to suppress undesired modes.

Figure 7 shows the dimensions of interest for the tapered rectangular cavity with a constant  $f_c$ . Here  $\delta$  is the distance from the probe to the radiating aperture,  $L$  is the probe length,  $d$  is the total depth of the cavity,  $a(z)$  is the width of the cavity in the x-direction, which now varies in the z-direction, and  $b = a_o/2.25$  and is constant in the z-direction. The width of the probe should be chosen to match the width of the cavity at  $z = \delta$ . Also  $d$  will be some fraction of the guide wavelength which now varies in the z-direction

$$a_1 = \frac{a_o}{\sqrt{\epsilon_r \mu_r}} \quad (2)$$

$$PW = \delta \tan \left( 180^\circ - \tan^{-1} \left( \frac{a_1}{2d} \right) \right) \quad (3)$$

$$\lambda_g = \frac{\lambda_o(c_f)}{\sqrt{(0.5\epsilon_r \mu_r - \left( \frac{\lambda_o(c_f)}{a_0 + a_1} \right)^2)}} \quad (4)$$

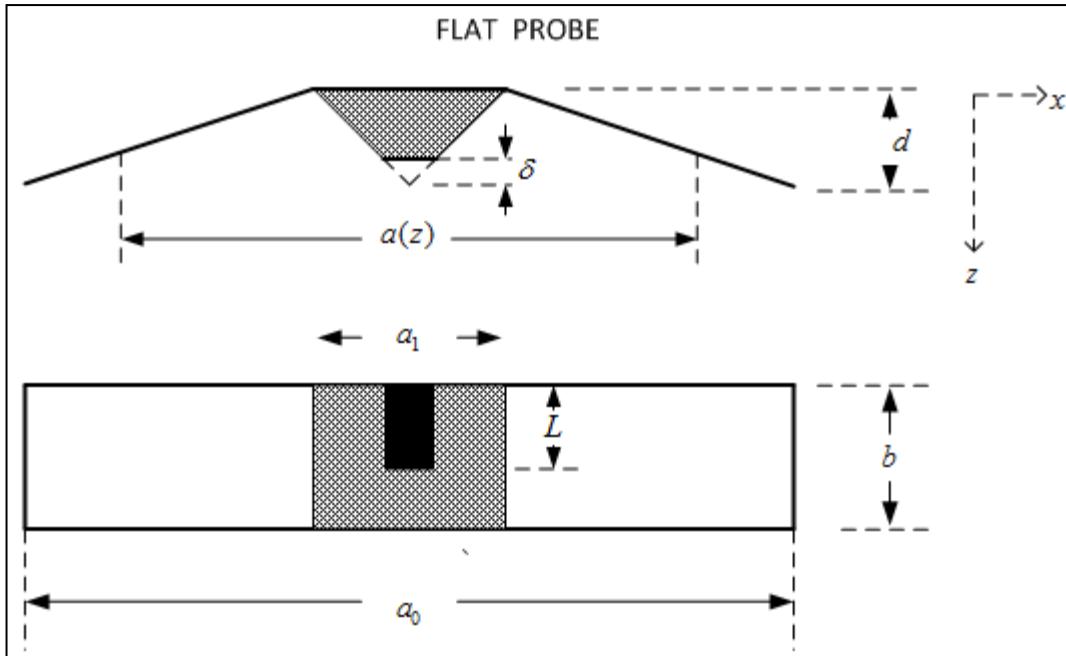


Figure 7. Illustration of the variable dimensions of a tapered rectangular cavity with constant cutoff frequency.

Equation 4 is truly the guide wavelength at  $z = d/2$ , where  $\lambda_0(c_f)$  is the free-space wavelength at the center frequency of the frequency band. This is simply used as an educated guess as the best way to determine the depth of  $d$  for the linear taper shown in figure 7. In fact, the linear taper is only used as a way to make other initial calculations simpler. In order to truly determine the shape of the taper, the transverse resonance of the tapered cavity must be calculated continuously across  $z$ . This is not included in this preliminary investigation.

### 3.1.1 Dielectric Materials

This section examines when the high index material has  $\epsilon_r = 10$  and  $\mu_r = 1$ . Figure 8 shows the realized gain across the entire band of interest. Figure 9 shows the return loss across the band of interest.

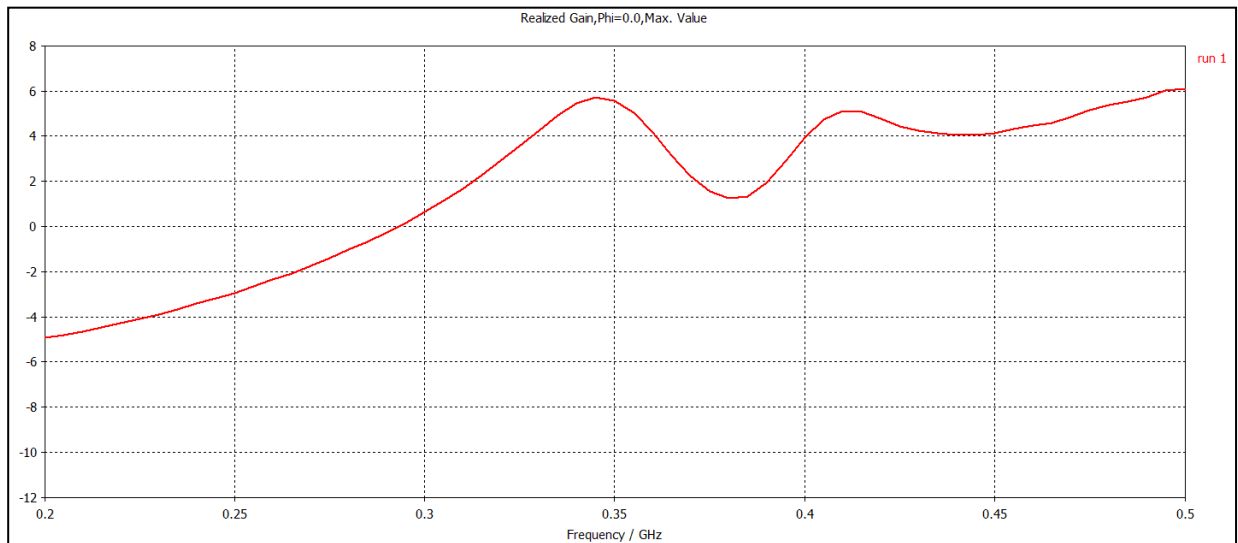


Figure 8. Realized gain with  $\epsilon_r = 10$  and  $\mu_r = 1$ .

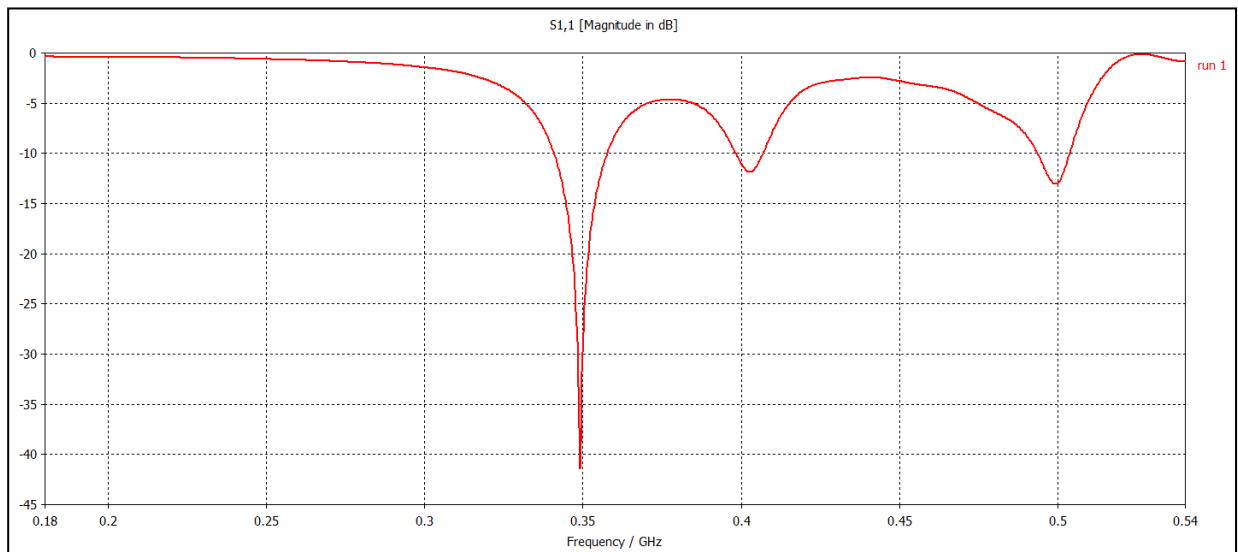


Figure 9. Return loss with  $\epsilon_r = 10$  and  $\mu_r = 1$ .

Figures 8 and 9 show that from 295–500 MHz we have a positive realized gain even though the return loss isn't particularly good over the entire range. This stems from the fact that the radiating aperture is nearly  $3 \text{ ft}^2$ , which becomes larger in terms of wavelength as frequency increases. To produce positive realized gain over the whole band, we would need to increase  $a_0$ , but the aperture size is already much larger than the desired  $2 \text{ ft}^2$ . This phenomenon of having a positive realized gain with a poor return loss is repeated throughout the following analyses and therefore is not being repeated. Any deviations from this established behavior are illustrated and noted.

### 3.1.2 Magnetic Materials

This section examines when the tapered high index material has  $\epsilon_r = 1$  and  $\mu_r = 10$ . Figure 10 shows the realized gain across the entire band of interest.

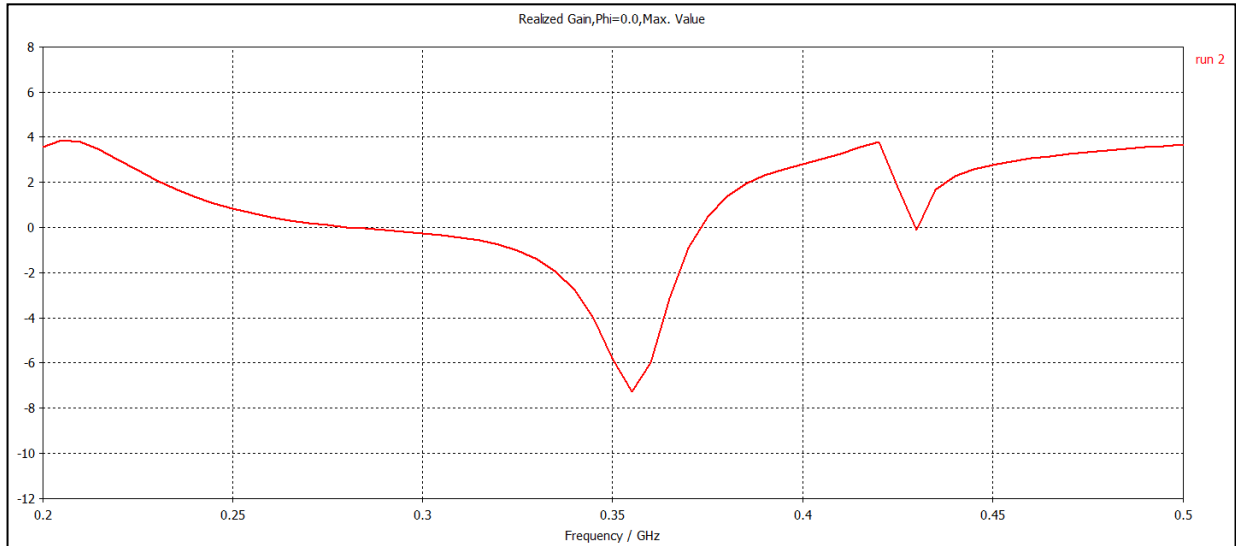


Figure 10. Realized gain with  $\epsilon_r = 1$  and  $\mu_r = 10$ .

Figure 10 shows a realized gain pattern almost mirroring that of figure 8. The realized gain for the magnetic material starts out positive and crosses 0 dB at just about the same point that the realized gain in the dielectric material becomes positive. While both seem to have a dip at 420 MHz, the dip of the dielectric material is much less pronounced and it also finishes much higher at the end of the frequency band.

### 3.1.3 Magneto-Dielectric Material

Since the dielectric material and magnetic material seem to cover different parts of the spectrum in term of positive realized gain, it is interesting to see how a magneto-dielectric material responds. Figure 11 shows the realized gain of a magneto-dielectric material with  $\epsilon_r = \sqrt{10}$  and  $\mu_r = \sqrt{10}$ . These values were chosen so that using equations 2–4, the cavity dimensions are the same as those listed in table 3.

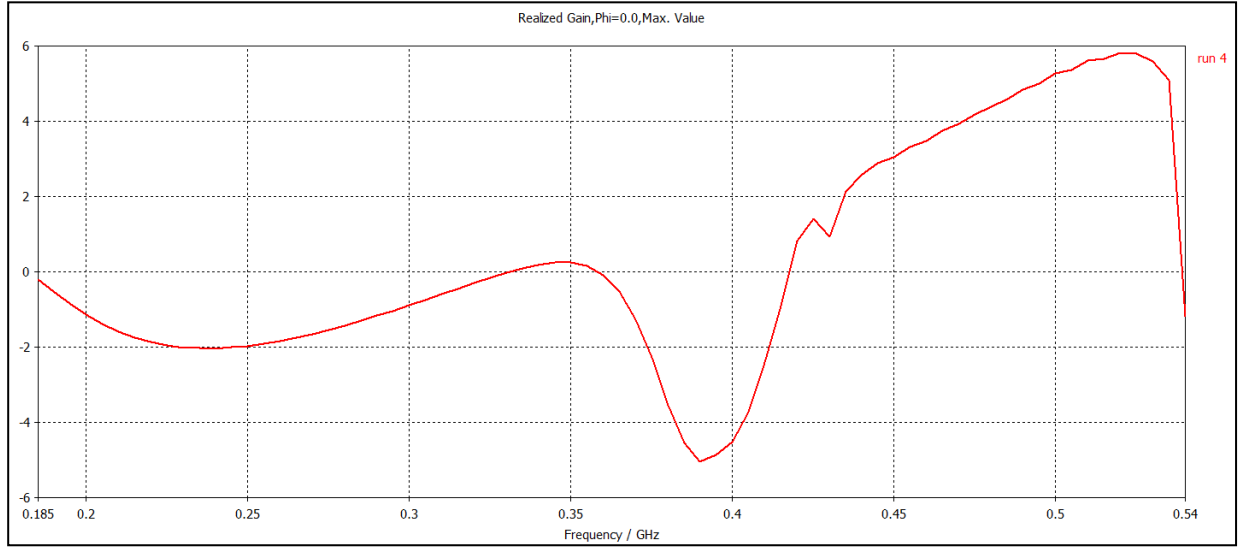


Figure 11. Realized gain with  $\epsilon_r = \sqrt{10}$  and  $\mu_r = \sqrt{10}$ .

Figure 11 shows a realized gain pattern that has negative realized gain over much of the band from 200–420 MHz. This seems to indicate that using magneto-dielectric materials is not as effective as a magnetic or dielectric material alone. Also, decreasing the values of  $\epsilon_r$  and  $\mu_r$  until they approached unity would, in fact, trend the curve in figure 11 toward that of the vacuum-filled cavity, but that goes against what we are trying to accomplish in reducing the cavity depth.

### 3.2 Anisotropic Materials

As we saw from the isotropic materials, the differences between dielectric, magnetic, and magneto-dielectric materials causes a positive gain response in different areas of the frequency band. However, we were not able to get a positive realized gain across the entire frequency band for a thin cavity, which requires relatively high values of  $\epsilon_r$  and  $\mu_r$ . Therefore, we look at the differences in various forms of anisotropic materials where  $\epsilon_r$  and  $\mu_r$  is controlled in all three Cartesian directions with the following tensors:

$$\epsilon_r = \begin{bmatrix} \epsilon_x & 0 & 0 \\ 0 & \epsilon_y & 0 \\ 0 & 0 & \epsilon_z \end{bmatrix} \quad \mu_r = \begin{bmatrix} \mu_x & 0 & 0 \\ 0 & \mu_y & 0 \\ 0 & 0 & \mu_z \end{bmatrix} \quad (5)$$

We examine how anisotropy in a single element of equation 5 affects the behavior of the far-field realized gain. All other tensor elements are set to unity in each case. In the following sections, we refer to the axis of analysis as the dominant axis. We continue to use the same forms of equations 2–4, where  $\epsilon_r$  and  $\mu_r$  are replaced with the tensor values of the dominant axis.

### 3.2.1 Dominant Axis in the X-Direction

Figure 12 shows the realized gain and return loss across the band for  $\epsilon_x = 10$  and the dimensions listed in table 3.

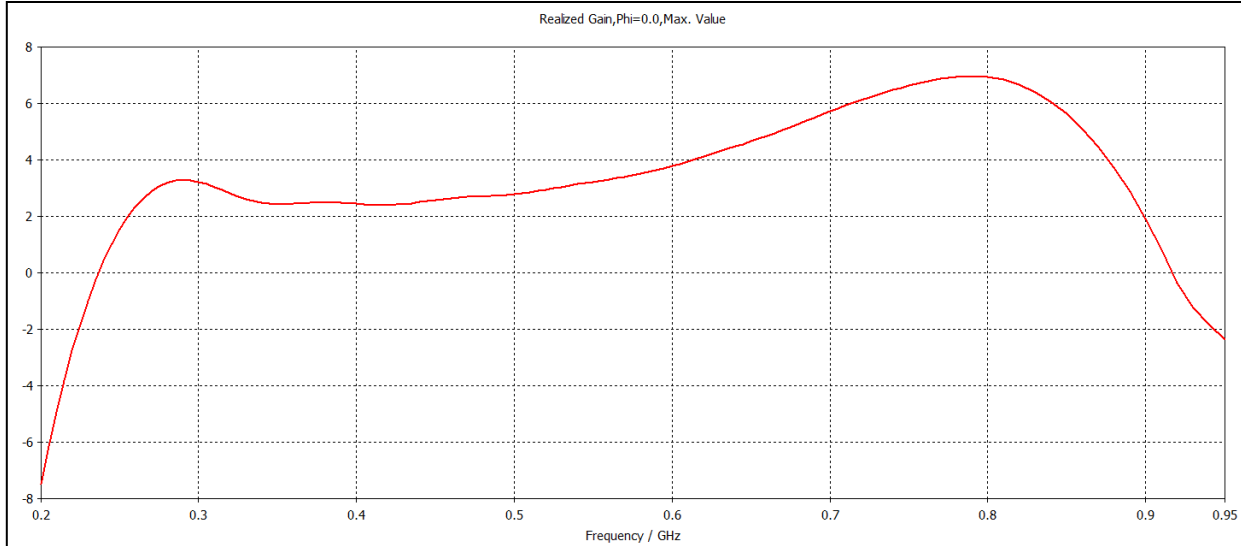


Figure 12. Realized gain with  $\epsilon_x = 10$ ,  $\epsilon_y = 1$ ,  $\epsilon_z = 1$ ,  $\mu_x = 1$ ,  $\mu_y = 1$ , and  $\mu_z = 1$ .

Figure 12 shows a positive realized gain from about 220–920 MHz. Figure 13 shows the realized gain and return loss across the band for  $\mu_x = 10$  and the dimensions listed in table 4.

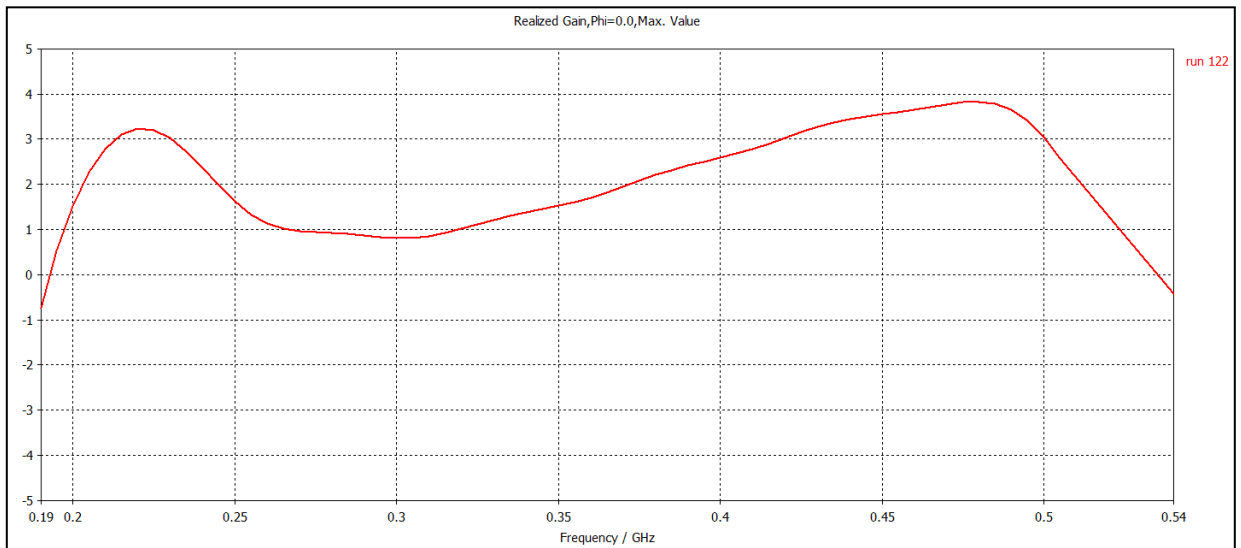


Figure 13. Realized gain for tapered cavity with dimensions given in table 4 with  $\epsilon_x = 1$ ,  $\epsilon_y = 1$ ,  $\epsilon_z = 1$ ,  $\mu_x = 10$ ,  $\mu_y = 1$ , and  $\mu_z = 1$ .

Table 4. Cavity dimensions for figure 8 in inches.

<b>a0</b>	<b>b</b>	<b>a1</b>	<b>fc (MHz)</b>	<b>d</b>	<b><math>\delta</math></b>	<b>PW</b>	<b>L</b>
26.25	11.7	8.3	225	4.2	0.29	1.0	8.5

Figure 13 shows positive realized gain across the entire band of interest. In fact, the band corresponding to positive realized gain is approximately a 340-MHz bandwidth, which exceeds the design goals of a 300-MHz bandwidth. The dimensions in table 4 also show that we were able to reduce the size of the aperture to 2.1 ft<sup>2</sup>, which is nearly in accordance with our 2-ft<sup>2</sup> requirement. In this instance, the dominant axis of the permeability tensor from equation 5 is in the same direction as the H-field at the aperture. Note that PW and the width of the top of the dielectric have been increased to 1.0 in so that it no longer strictly adheres to equation 3. This was done to help bring up the trough seen from 250–375 MHz, to some degree.

Since this is the only configuration to achieve a positive realized gain across the entire frequency band of interest, we want to look at how increasing the values of  $\mu_x$  may help to reduce the cavity depth  $d$  while still maintaining a positive realized gain. Figure 14 shows the realized gain across the band for  $\mu_x = 15$  and  $\mu_x = 20$ . Figure 15 shows the VSWR across the band for  $\mu_x = 15$  and  $\mu_x = 20$ . The cavity dimensions are listed in table 5.

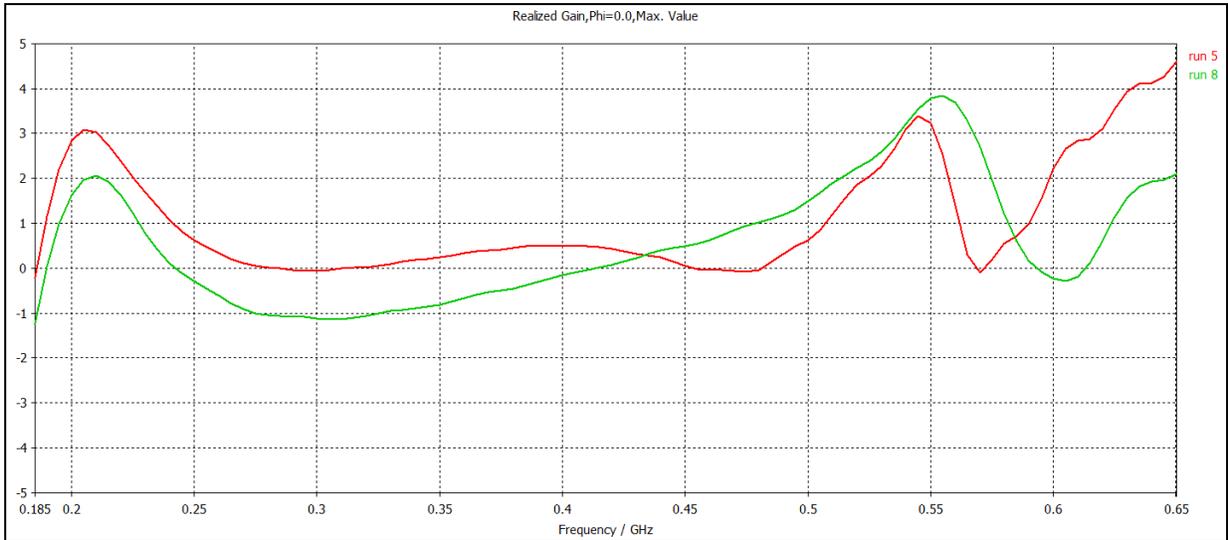


Figure 14. Realized gain with  $\epsilon_x = 1$ ,  $\epsilon_y = 1$ ,  $\epsilon_z = 1$ ,  $\mu_y = 1$ , and  $\mu_z = 1$ . Run 5 has  $\mu_x = 15$  while run 8 has  $\mu_x = 20$ .

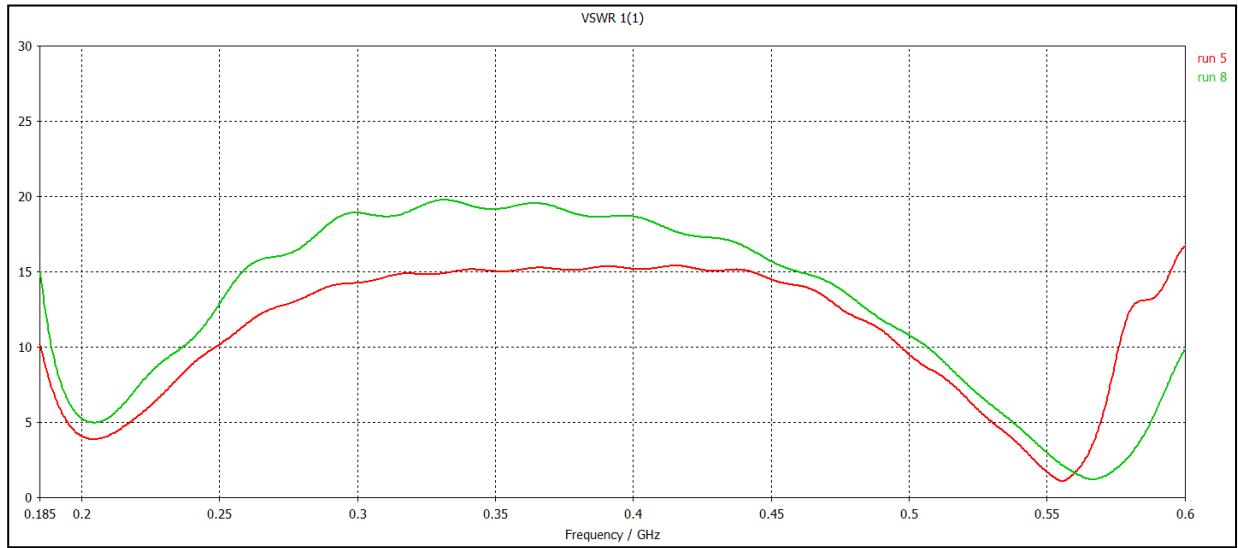


Figure 15. VSWR with  $\epsilon_x = 1$ ,  $\epsilon_y = 1$ ,  $\epsilon_z = 1$ ,  $\mu_y = 1$ , and  $\mu_z = 1$ . Run 5 has  $\mu_x = 15$  while run 8 has  $\mu_x = 20$ .

Table 5. Cavity dimensions for figures 11 and 12 in inches.

Run	$\mu_x$	$a_0$	$b$	$a_1$	$f_c$ (MHz)	$d$	$\delta$	PW	L
5	15	32.8	14.6	8.5	180	3.2	0.25	1.0	8.5
8	20	32.8	14.6	7.3	180	2.8	0.25	1.0	8.5

Run 5 of figure 14 shows positive realized gain across the entire band of interest when  $\mu_x = 15$ . The band corresponding to positive realized gain exceeds a 450-MHz bandwidth. This far outstrips the bandwidth of figure 13 when  $\mu_x = 10$ . However, it comes at the cost of increasing the aperture size from 2.1 ft<sup>2</sup> to 3.3 ft<sup>2</sup>, which is undesirable. We were able to achieve an inch reduction in depth from when  $\mu_x = 10$ , which gets us closer to our goal of 2 in. Here we see that there is a definite tradeoff between reductions in depth versus an increase in aperture size. To demonstrate this point run 8 shows a resonant cavity with the same aperture size but with  $\mu_x = 20$ . Here we see a loss of 1 dB across the 200–400 MHz band versus run 5. Again we may be able to make up for this by increasing the aperture size further, but this becomes redundant since we have already exceeded our desired aperture size by more than 1 ft<sup>2</sup>. Furthermore, we were only able to reduce the depth another 0.4 in by increasing  $\mu_x$  so there is a law of diminishing returns in depth reduction versus the required increase in aperture size.

This phenomenon is better explained by figure 15 which shows the VSWR of the loaded cavity with dimensions given in table 5. The high VSWR of both runs indicates a very poor match on the order of  $-2$  dB or worse over much of the band. This is why such a large aperture is necessary to achieve a positive gain in run 5 and an even larger aperture would be necessary for run 8. This indicates that increasing permeability or permittivity in any direction (including the

isotropic cases) yields a worse match at the input of the coaxial feed. We are sacrificing match to decrease cavity depth in these cases and that in turn decreases the realized gain even for lossless materials. Non-traditional methods beyond those described in reference 6 need to be investigated in order to create a better broadband match. This, in turn, allows us to decrease the aperture size as well as continue to decrease the cavity depth with more hope of broadband positive realized gain.

### 3.2.2 Dominant Axis in the Y-Direction

Figure 16 shows the realized gain and return loss across the band for  $\epsilon_y = 10$  and the dimensions listed in table 3.

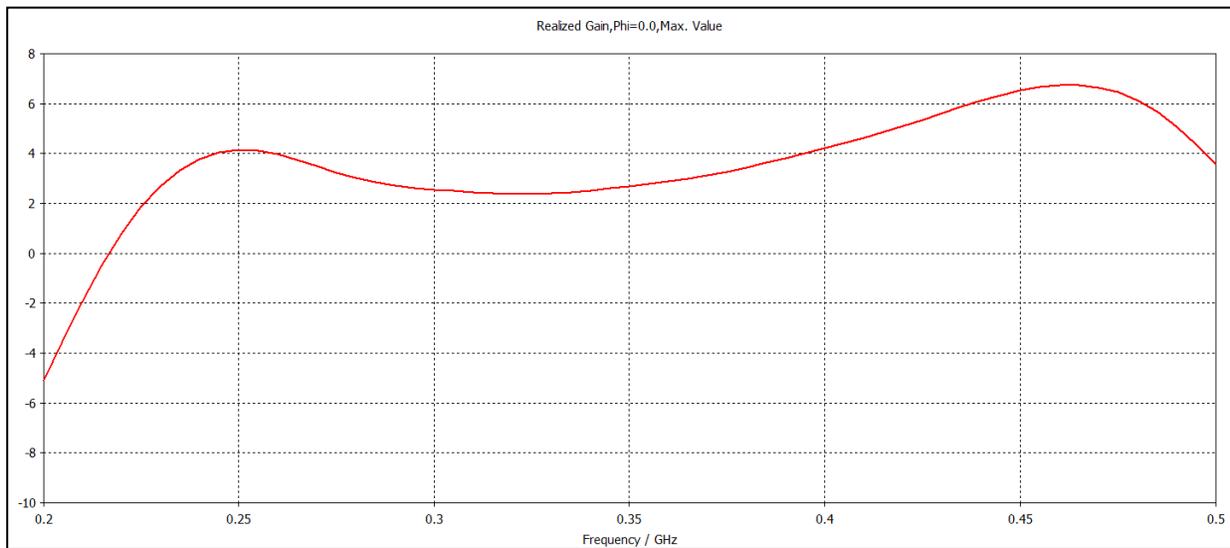


Figure 16. Realized gain with  $\epsilon_x = 1$ ,  $\epsilon_y = 10$ ,  $\epsilon_z = 1$ ,  $\mu_x = 1$ ,  $\mu_y = 1$ , and  $\mu_z = 1$ .

Figure 16 shows a positive realized gain from about 215–500 MHz, but again with a radiating aperture of nearly 3 ft<sup>2</sup>. In this instance the dominant axis of the permittivity is aligned in the same direction as the E-field at the aperture, and we see an increase in realized gain over figures 13 and 14 over the entire frequency range except from about 200–225 MHz. In a later section, we try to take advantage of both of these phenomena.

Figure 17 shows the realized gain and return loss across the band for  $\mu_y = 10$  and the dimensions listed in table 3.

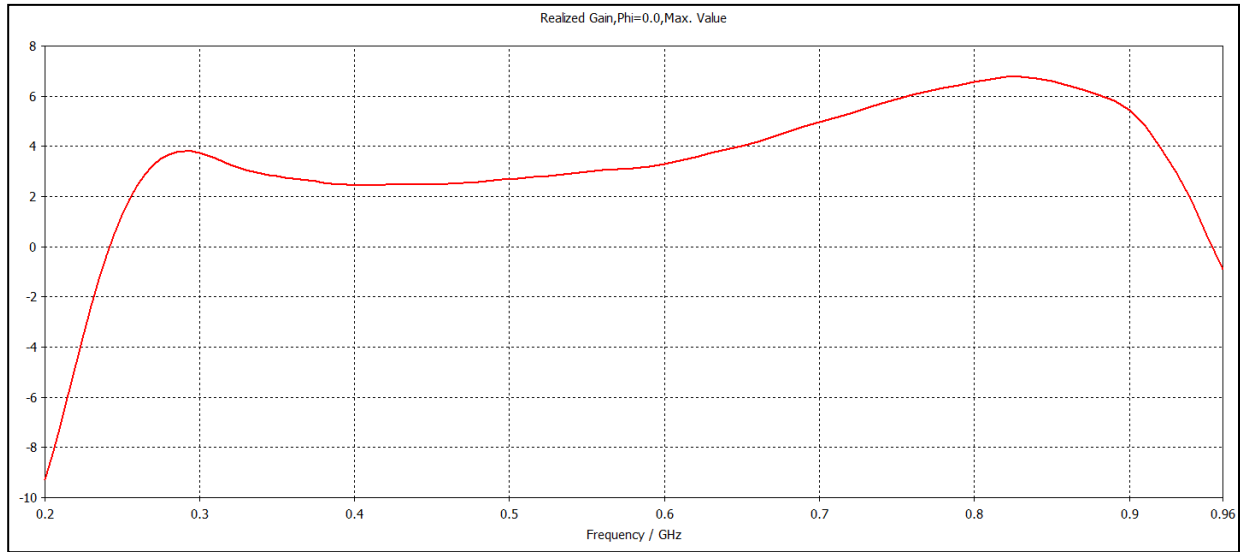


Figure 17. Realized gain with  $\epsilon_x = 1$ ,  $\epsilon_y = 1$ ,  $\epsilon_z = 1$ ,  $\mu_x = 1$ ,  $\mu_y = 10$ , and  $\mu_z = 1$ .

Figure 17 shows a positive realized gain from about 240–955 MHz, but again with a radiating aperture of nearly 3 ft<sup>2</sup>. In this instance, the dominant axis of the permeability is aligned in the same direction as the E-field at the aperture. We see a similar plot as for when  $\epsilon_x = 10$  except with a higher gain.

### 3.3.3 Dominant Axis in the Z-Direction

Figure 18 shows the realized gain and return loss across the band for  $\epsilon_z = 10$  and the dimensions listed in table 3.

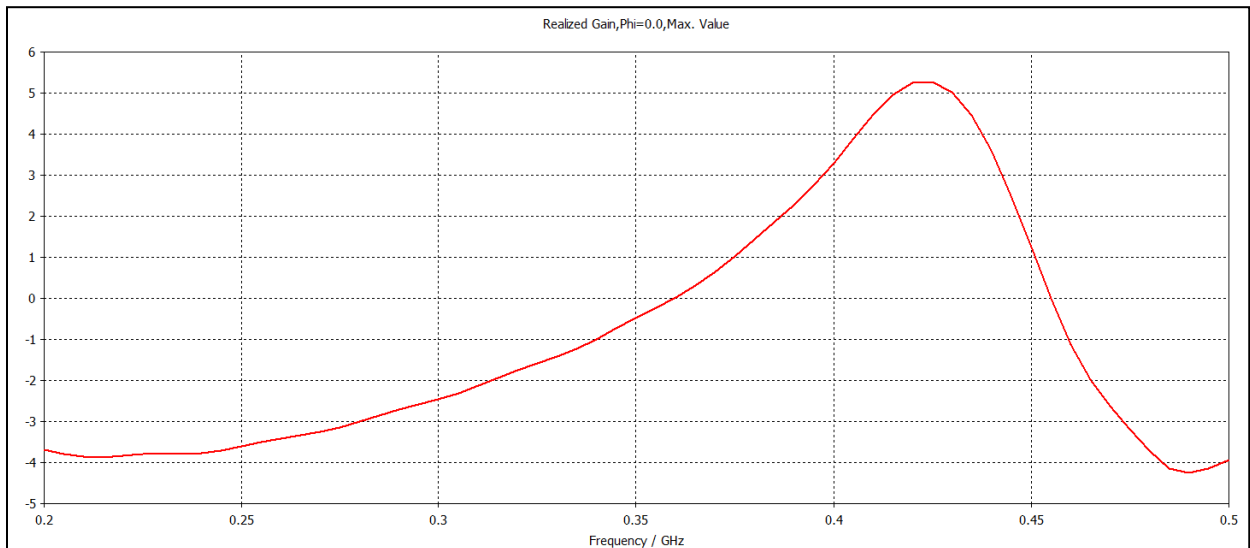


Figure 18. Realized gain with  $\epsilon_x = 1$ ,  $\epsilon_y = 1$ ,  $\epsilon_z = 10$ ,  $\mu_x = 1$ ,  $\mu_y = 1$ , and  $\mu_z = 1$ .

Figure 18 shows a positive realized gain from about 360–455 MHz. This is the narrowest band of positive realized gain we have seen thus far and probably doesn't warrant further investigation.

Figure 19 shows the realized gain and return loss across the band for  $\mu_z = 10$  and the dimensions listed in table 3.

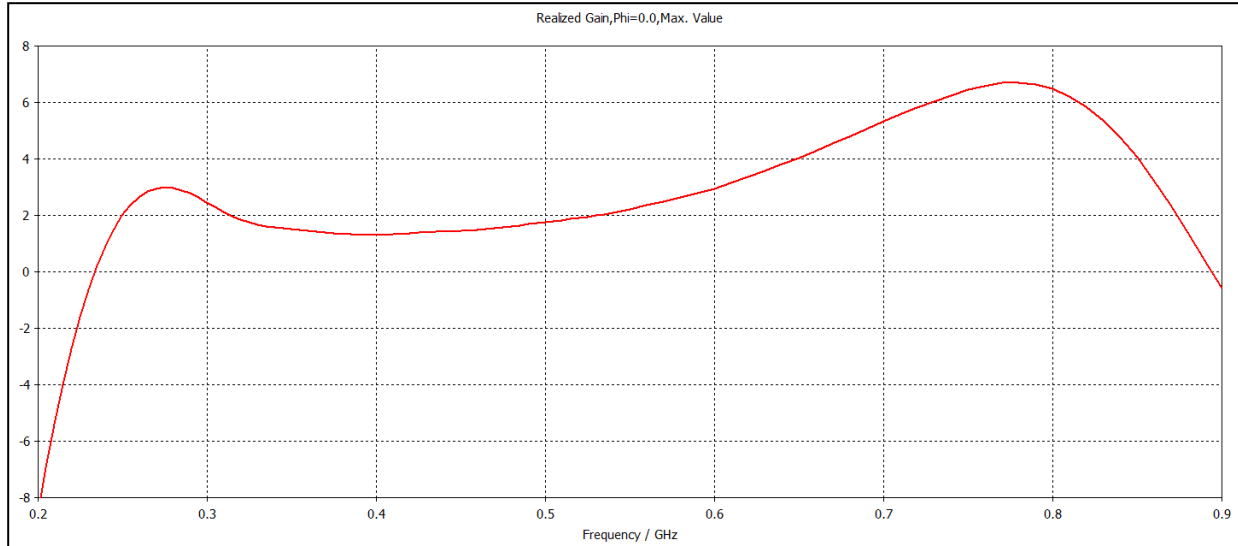


Figure 19. Realized gain with  $\epsilon_x = 1$ ,  $\epsilon_y = 1$ ,  $\epsilon_z = 1$ ,  $\mu_x = 1$ ,  $\mu_y = 1$ , and  $\mu_z = 10$ .

Figure 19 shows a positive realized gain from about 235–900 MHz. This is very similar to the behavior when  $\epsilon_x = 10$  and also when  $\mu_y = 10$ .

### 3.4 Dominant Axes in the $\mu_x$ and $\epsilon_y$ Directions

Since figure 16 ( $\epsilon_y = 10$ ) shows a higher and flatter realized gain response between 225–500 MHz than figure 13 ( $\mu_x = 10$ ), we would like to see what the result of combining these two phenomena would be. Figure 20 shows the realized gain and return loss across the band for  $\mu_x = 10$  and  $\epsilon_y = 10$  for the dimensions listed in table 3.

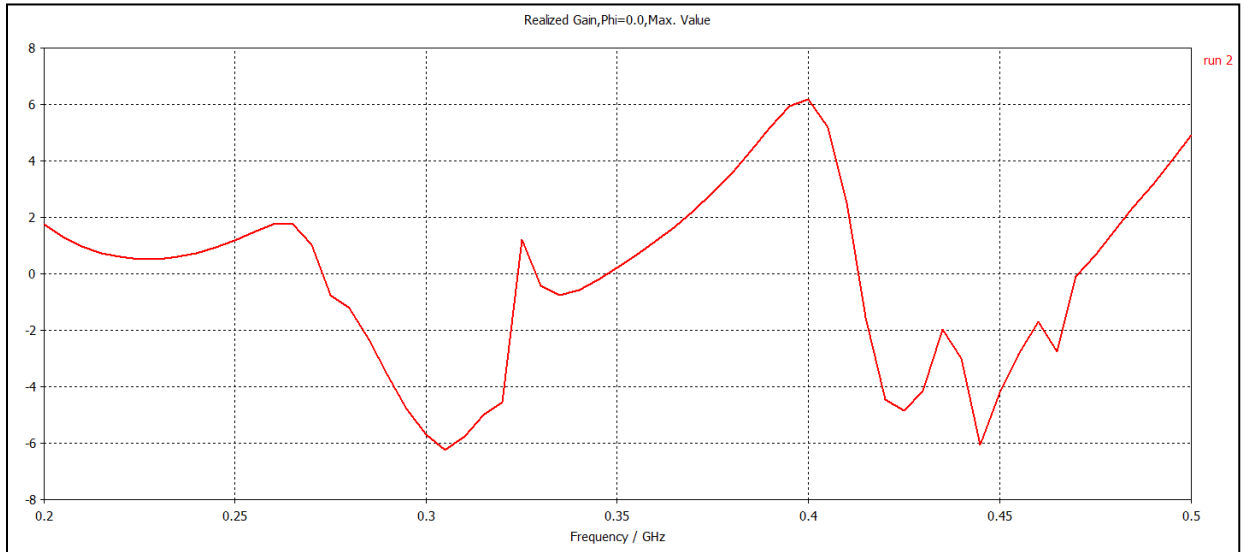


Figure 20. Realized gain with  $\epsilon_x = 1$ ,  $\epsilon_y = 10$ ,  $\epsilon_z = 1$ ,  $\mu_x = 10$ ,  $\mu_y = 1$ , and  $\mu_z = 1$ .

Figure 20 shows that except for a very narrowband region from 350–400 MHz the realized gain is lower than for either the  $\mu_x = 10$  or  $\epsilon_y = 10$  case individually. This is a similar phenomenon as we saw with the isotropic magneto-dielectric material.

### 3.5 Dominant Axes in the $\mu_x$ and $\mu_z$ Directions

Since figure 19 ( $\mu_z = 10$ ) shows a higher and flatter realized gain response between 250–500 MHz than figure 14 ( $\mu_x = 15$ ), we would like to see what the result of combining these two phenomena would be. Figure 21 shows the realized gain and return loss across the band for  $\mu_x = 15$  and  $\mu_z = 10$  for the dimensions listed in table 5 at  $f_c = 180$  MHz. The only variable here is  $f_c$  and it is important to note that as  $f_c$  increase the size of  $a_0$ ,  $a_1$ , and  $b$  will decrease thus reducing aperture size.

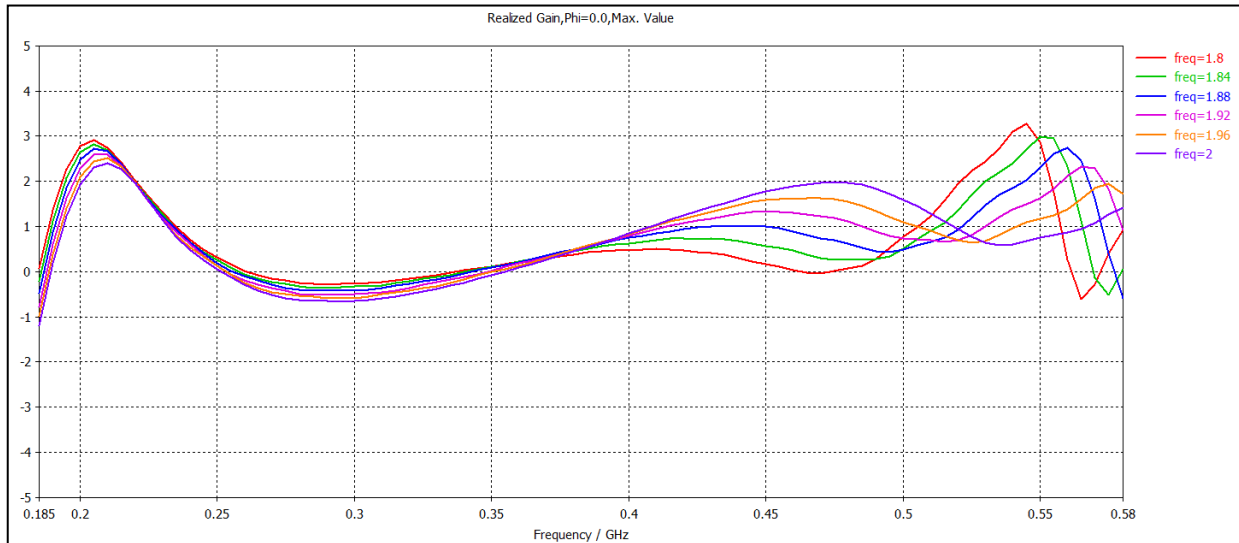


Figure 21. Realized gain with  $\epsilon_x = 1$ ,  $\epsilon_y = 1$ ,  $\epsilon_z = 1$ ,  $\mu_x = 15$ ,  $\mu_y = 1$ , and  $\mu_z = 10$ .

Figure 21 has the same shape as figure 14 although the realized gain falls below 0 dB between 250–350 MHz. The multiple runs show a progression in  $f_c$  that illustrates how as we increase the size of the aperture we increase the realized gain over 250–350 MHz, but sacrifice realized gain from 450–500 MHz. Decreasing  $f_c$  below 180 MHz may eventually provide a positive realized gain at the lower frequencies, but will then create a new problem from 450–500 MHz. This further emphasizes the fact that the only way to address this problem would be to introduce additional matching elements to the feed to make up for this inability to make up for poor realized gain through aperture size alone.

## 4. Conclusions

This report examined the use of high index materials to reduce the thickness of an aperture backed by a tapered rectangular resonant cavity. Both isotropic and anisotropic materials were analyzed for various cavity depths and aperture sizes. Using traditional feeding techniques, we were able to show that a vacuum-filled cavity produced a good realized gain and input match from 200–500 MHz. However, the large thickness of the cavity (10.2 in) makes it unusable in low profile applications.

Using high index materials to load the cavity, we showed that we were able to reduce cavity thickness by more than a factor of 2.5 in the worst-case scenario and a factor of more than 3 in the best-case scenario. In order to restrict the propagation of higher order modes within the cavity, both the cavity structure itself and the high index material have to be tapered to provide a constant cutoff frequency.

Looking at dielectric, magnetic, and magneto-dielectric materials showed that the magneto-dielectric materials were the worst performers in all cases. The isotropic case study showed that while both dielectric and magnetic materials achieved a positive realized gain over parts of the band neither covered the entire 300-MHz bandwidth. The anisotropic case study showed that individually controlling the permittivity and permeability in all three Cartesian directions yielded much better results. However, the only case that produced positive realized gain over the entire band was for a magnetic material with the dominant tensor direction aligned parallel to the H-field at the aperture. In this case, we were able to reduce the depth of the cavity to 3.2 in and the size of the aperture to 2.1 ft<sup>2</sup>. While these are encouraging results, by improving the match at the input we believe that the realized gain can be improved further while continuing to reduce the depth of the cavity.

---

## 5. Path Forward

---

1. Investigate additional matching/feeding techniques that will lower the broadband VSWR of the tapered cavity loaded with high index anisotropic materials.
2. Investigate other cavity shapes, such as conical, that may be used to increase the operational bandwidth or increase the realized gain.
3. Derive the anisotropic transverse resonance condition for a tapered cavity to determine the optimal shape of the taper for the high index material within.
4. Analyze the effects of lossy high index material on the far-field radiation characteristics of the cavity backed aperture.
5. Compare results using the infinite conducting flange approximation for those of a finite flange and determine the size of the flange needed.
6. Taking steps 1–5 into account determine the thinnest cavity with the smallest aperture size that produces a positive gain over the 200–500 MHz frequency band and identify the type of material that achieves this. Increase this bandwidth potential if at all possible.

---

## 6. References

---

1. *Antenna Handbook* (Vols. I and Vols. II), Van Nostrand Reinhold, New York, 1993.
2. Amitay, N.; Gallindo, V.; Wu, C. P. *The Theory and Analysis of Phased Array Antennas*. New York: Wiley-Interscience, 1972.
3. Aidet, J. et al. Electrical Characteristics of Waveguide Applicators for Medical Applications. *Journal of Microwave Power* 15 (3), 177–186.
4. Nikita, K.; Uzunoglu, N. K. Coupling Phenomena in Concentric Multi-applicator Phased Array Hyperthermia Systems. *IEEE Trans. Microwave Theory Tech.* **Jan. 1996**, 44 (3), 65–74, Jan. 1996.
5. Williamson, A. G. Analysis and Modeling of a Coaxial-line/Rectangular-waveguide Junction. *IEEE Proceedings (Microwaves, Optics, and Antennas)* **October 1982**, 129, Issue 5.
6. Wade, P. *Rectangular Waveguide to Coax Transition Design*. QEX, November/December 2006.

1 DEFENSE TECHNICAL  
(PDF) INFORMATION CTR  
DTIC OCA

2 DIRECTOR  
(PDFS) US ARMY RESEARCH LAB  
RDRL CIO LL  
IMAL HRA MAIL & RECORDS MGMT

1 GOVT PRINTG OFC  
(PDF) A MALHOTRA

5 DIRECTOR  
(PDFS) US ARMY RESEARCH LAB  
ATTN RDRL SER M G MITCHELL  
ATTN RDRL SER M E ADLER  
ATTN RDRL SER M S WEISS  
ATTN RDRL SER M A ZAGHLOUL  
ATTN RDRL SER M K COBURN